Development of a new cold hardiness prediction model for grapevine using phased integration of acclimation and deacclimation responses

Al P. Kovaleski[1,*], Michael G. North[1], Timothy E. Martinson[2], Jason P. Londo[2,*]

[1]Department of Horticulture, University of Wisconsin–Madison, Madison, WI 53706, USA

[2]School of Integrative Plant Science, Cornell AgriTech, Cornell University, Geneva, NY 14456, USA

[*]Authors for correspondence:

AP Kovaleski: al.kovaleski@wisc.edu

JP Londo: jpl275@cornell.edu

Highlights

- Multi-year cold hardiness data from three grapevine cultivars were used for modeling
- Cold hardiness was modeled based on daily temperature and accumulated chill
- Phased acclimation and deacclimation processes result in cold hardiness predictions
- The new model was compared to the currently available model for grapevines
- The model proposed here outperforms the currently available model

Abstract

Cold injury limits distribution of perennial agricultural crops, though replacement of plants and other management practices may allow for some damage tolerance. However, winter damage to crops such as grapevines (*Vitis* spp.) can result in losses in yield the following year if buds are damaged, but over many years when vines must be replaced and reach maturity before fruiting. Despite risks, grapevines are cultivated at the edge of permissible climate and rely on cold hardiness monitoring programs to determine when cold damage mitigation and management practices are required. These monitoring programs represent a critical, but laborious process for tracking cold hardiness. To reduce the need for continuous monitoring, a model (WAUS.2) using cold hardiness data collected over many years from Washington state, USA, growers was published in 2014. Although the WAUS.2 model works well regionally, it underperforms in other regions. Therefore, the objective of this work was to develop a new model (NYUS.1) that incorporates recent knowledge of cold hardiness dynamics for better prediction outcomes. Cold hardiness data from *V. labruscana* 'Concord', and *V. vinifera* 'Cabernet Sauvignon' and 'Riesling' from Geneva, NY, USA were used. Data were separated in calibration (~2/3) and validation (~1/3) datasets. The proposed model uses three functions to describe acclimation, and two functions to describe deacclimation, with a total of nine optimized parameters. A shared chill response between acclimation and deacclimation provides a phased integration where acclimation responses decrease over the course of winter and are overcome by deacclimation. The NYUS.1 model outperforms the WAUS.2 model, reducing RMSE by up to 37% depending on cultivar. The NYUS.1 model also tends to be more conservative in its prediction, slightly underpredicting cold hardiness, as opposed to the overprediction from the WAUS.2 model. Some optimized parameters were shared between cultivars, suggesting conserved physiology was captured by the new model.

Keywords

Grapevine, *Vitis*, cold hardiness, model, differential thermal analysis

1. Introduction

One of the most important abiotic stresses limiting the distribution of plants worldwide is low winter temperatures. Single freezing events can effectively eliminate plant populations, thus limiting the cold range edge of native plants (Körner, 2021). Perennial agricultural plants are often introduced beyond their native cold range limits and therefore have higher risk of cold injury during winter (Hänninen, 2013). This is the case for grapevines (*Vitis* spp.), especially domesticated European grapevines (*V. vinifera*), in northern regions within the United States and in Canada, where low temperatures during the dormant season in winter are a limiting factor. In these agricultural systems, injured or dead plants can be replaced, although this increases production costs and can create gaps or delays in production. Therefore, understanding and predicting cold hardiness of perennial plants can be helpful in determining management practices and site selection based on winter survival.

Domesticated European grapevines are native to the Mediterranean yet are cultivated on all continents except Antarctica. Within the US, New York state is the third largest grape producer in the US (USDA, 2019), growing grapevines in significantly colder conditions than that of the larger two producing states (California and Washington), and colder than some regions with which it shares latitudes within Europe, such as northern Spain, southern France, and central Italy. Viticulture in New York relies on the proximity to large bodies of water (e.g., Lake Erie, Lake Ontario, the Finger Lakes, Atlantic Ocean) to help buffer low temperatures during winter, thus allowing cultivation of *V. vinifera* grapevines, which are generally less cold hardy than American species (e.g., *V. labrusca*, *V. riparia*) and hybrid varieties (Londo and Kovaleski, 2017). Winter survival of mixed buds in grapevines is required for production of grapes in the following growing season. These buds are formed during summer and must remain dormant and develop cold hardiness throughout fall to survive low temperatures in winter before resuming growth in spring. The ability to predict bud cold hardiness would allow growers to monitor conditions and decide when it may be necessary to evaluate winter bud injury, particularly in currently cold growing regions, but accurate predictions could also be used to evaluate current suitability for expansion into other areas, or for identifying regional suitability changes as climate changes. While climate predictions suggest winter temperatures will rise, more erratic climate is also expected with large swings between warm temperatures and acute low temperatures (IPCC, 2022). As cold damage mitigation tools are developed, accurate predictions of cold hardiness are also needed to assess necessity and timing of deployment of these methods (Li and Dami, 2016; Kovaleski and Londo, 2019). Therefore, accurate

cold hardiness models can help evaluate the future of viticulture in cold climates from a winter survival standpoint.

Dormancy and cold hardiness are separate but concomitant processes within a plant (Arora et al., 2003; Kovaleski, 2022). Both processes are required for survival of low temperatures during the cold season in subtropical and temperate environments but appear to respond to slightly different environmental cues. Dormancy establishment in grapevines typically occurs in response to shortening photoperiod in late summer and fall (Fennel and Hoover, 1991) but other environmental factors can also play a role [e.g., drought (Shellie et al., 2018)]. Dormancy progression is then modulated by exposure to low temperatures (chilling), transitioning from a warm temperature non-responsive (endodormancy) to a responsive phase (ecodormancy), from which plants are released from upon return of warm temperatures in spring (Lang et al., 1987).

Cold hardiness usually presents a U-shape pattern during the progression from fall to winter to spring with three distinct phases (Ferguson et al., 2011; Ferguson et al., 2014; Cragin et al., 2017; Londo and Kovaleski, 2017; Kovaleski, 2022). In the fall, acclimation leads to gains in cold hardiness of grapevine buds through the establishment and enhancement of supercooling. In mid-winter, buds reach maximum cold hardiness and maintain high levels of cold hardiness depending on environmental cues. Finally, in late winter and early spring as warm temperatures return, deacclimation leads to loss of cold hardiness – though reacclimation is possible upon return of low temperatures. Photoperiod alone is unable to elicit significant gains in cold hardiness (Fennel and Hoover, 1991). While some authors have indicated that only the synergistic effect of short photoperiod and low temperatures can induce deep cold hardiness (Schnabel and Wample 1987), temperature effects appear to be the largest contributors to cold hardiness levels of grapevine buds, and models solely based on temperature have shown to produce good regional predictions (Ferguson et al., 2011; Ferguson et al., 2014; North et al., 2021).

Dormancy directly affects cold hardiness dynamics. During the endodormant period, in the fall and early winter, buds respond to low temperatures to gain cold hardiness. The ability to gain cold hardiness appears to decrease as chilling accumulates and buds transition to ecodormancy (Ferguson et al., 2011; Ferguson et al., 2014; North et al., 2021). The inverse seems to happen with regards to warm temperatures: a bud's deacclimation responsiveness increases as chilling accumulates (Ferguson et al.

2011, 2014; Cragin et al., 2017; Kovaleski et al., 2018; North et al., 2021; Kovaleski, 2022). Therefore, acknowledging dormancy dynamics is necessary for predicting cold hardiness.

Currently, the most widely used model for predicting grapevine bud cold hardiness was developed using cold hardiness data from Washington state based on *V. vinifera* 'Cabernet Sauvignon', 'Chardonnay', and *V. labruscana* 'Concord' (Ferguson et al., 2011), and was later enhanced and further expanded to add twenty other cultivars (Ferguson et al., 2014). Here we propose a new nomenclature for these models, using the region and country of development, as well as a version number. Therefore, from here on the models proposed by Ferguson and collaborators are referred to as WAUS.1 (Ferguson et al., 2011) and WAUS.2 (Ferguson et al., 2014). The WAUS.2 model has also been recently adapted for cold climate interspecific hybrids grown in a different environment (North et al., 2021). However, as indicated by the original authors, local adaptation of the model may be required given the specific climate in which it was developed. Indeed, the model does not produce reliable results in viticultural regions in the Eastern United states, including the state of New York. This is likely a consequence of trade-offs among three dimensions in models: accuracy, realism, and generality (Levins, 1966; Levins, 1968). Accuracy represents the fit between predictions and observations, realism refers to causally appropriate internal model processes, and generality represents robust applicability across space and/or time (Kramer et al., 2002). A model will ideally maximize all accuracy, realism, and generality simultaneously; however, in practice, model developers must identify an optimal point among the three dimensions that matches the overall aim of a model (Hänninen, 2016). In the case of the WAUS.2 model, accuracy was prioritized over realism and generality. Recent studies of dormancy related to cold hardiness have shown that some of the parameters used in the model, such as the linear response to temperature and the discrete change in responses by the vines based on dormancy status do not accurately describe the nature of the process (Kovaleski et al., 2018; North et al., 2022). In fact, linear responses to temperature have been related to errors in predictions of spring phenology as well (Wolkovich et al., 2021).

The objective of this study was to develop a new model (NYUS.1) for cold hardiness prediction of grapevine buds with greater accuracy for the Eastern United States and other viticultural regions more broadly. To do so, we use a medium-term dataset comprised of three cultivars: *V. labruscana* 'Concord', and *V. vinifera* 'Cabernet Sauvignon' and 'Riesling'. The choice of cultivars was made based on availability of data (partially due to regional relevance), and variability in responses. The new model expands from previously empirically determined concepts of deacclimation in response to chilling and

forcing temperatures (Kovaleski et al., 2018; Kovaleski, 2022; North et al., 2022), thus with increased realism, and incorporates theoretical derivation of acclimation functions based on preliminary experimental data to predict cold hardiness with field-based temperature data.

2. Materials and Methods

2.1. Cold hardiness data. Bud cold hardiness data from three cultivars were used: *V. labruscana* 'Concord', *V. vinifera* 'Cabernet Sauvignon', and *V. vinifera* 'Riesling' (from here on referred to by cultivar name only). Buds were collected from vineyards located in Geneva, NY, throughout multiple dormant seasons in varying numbers depending on cultivar (for details, see **Supplementary Table S1**). Cold hardiness was measured using differential thermal analysis (DTA) (Wolf and Pool, 1987; Mills et al., 2006; Ferguson et al., 2011; Ferguson et al., 2014; Londo and Kovaleski, 2017, North et al., 2021). Briefly, for DTA, buds are placed on thermoelectric modules connected to a datalogger and placed into a programmable freezer which can gradually lower temperature over time. Once intracellular water freezes, heat release is recorded as a low temperature exotherm (LTE) and signifies the temperature of death for any given bud (see Mills et al., 2006 for additional details). The number of buds used to measure cold hardiness for each cultivar on each sampling date varied between 5 and 30 buds (although number of recovered peaks may have been lower). For model development, average LTE values for each sampling date were used.

Eight seasons of data are available for 'Concord', five for 'Cabernet Sauvignon', and nine for 'Riesling'. The number of observations in each season varied based on cultivar, length of the season, and research program. For some seasons, more than one program collected data independently, but data were combined for modeling without using lab as a factor.

2.2. Weather data. Weather data were obtained from the Network for Environment and Weather Applications (NEWA; www.newa.cornell.edu). Hourly data were downloaded from which daily maximums and minimums were extracted for model development.

2.3. Data analyses. All data were analyzed with R (ver. 4.1.2; R Core Team, 2021) within R Studio (RStudio Team, 2021). Chill accumulation was calculated from hourly temperature data for each winter

based on the dynamic model (chill portions; Fishman et al., 1987a; Fishman et al., 1987b) using the chillR package (Luedeling, 2020). Three inputs were then used for model development, daily maximum (T_{max}) and minimum temperatures (T_{min}), and chill accumulation (*chill*, which is a function of temperature).

2.4. Model development. The model presented here is based on a generalized function for cold hardiness (*CH*) from Kovaleski (2022) where the *CH* at any time t_i during the dormant season is a result of the integration of separate acclimation and deacclimation processes occurring starting from bud set to t_i:

$$CH_{t_i} = CH_{bud\ set} + \int_{bud\ set}^{t_i} Acclimation\ dt + \int_{bud\ set}^{t_i} Deacclimation\ dt \quad [Eq.1]$$

where $CH_{bud\ set}$ is the cold hardiness of buds as they set and mature in late summer and fall, which is a characteristic of the tissues, and *Acclimation* and *Deacclimation* are comprised of functions described below. Here, *Acclimation* and *Deacclimation* are integrated over daily time steps for *t*, but both are functions of temperature, either directly or indirectly through *chill*. However, field temperatures are themselves a function of time.

2.4.1. For ***Acclimation***, three functions were used and are based on expectations of the responses (visual representations of these are presented in **Figs. 1A-D**). First, a function is used to describe what is the maximum temperature below which any acclimation occurs as a response to chilling accumulation [the acclimation temperature threshold ($T_{th_{acc}}$)]:

$$T_{th_{acc}}(chill) = T_{th_{low}} + {(T_{th_{high}} - T_{th_{low}})}\Big/{1 + e^{[b\ (\ln(chill) - \ln(c)]}} \quad [Eq.2]$$

where the temperature threshold for acclimation decreases from a high threshold ($T_{th_{high}}$) at low chill accumulations to a low threshold ($T_{th_{low}}$) at high chill accumulations; *b* is the slope associated with how quickly the decrease occurs, and *c* is the inflection point of the log logistic curve (**Fig. 1A**). This decrease in temperature threshold represents physiological changes during chill accumulation and dormancy progression affecting the directionality of the cold hardiness dynamics process: at high chill accumulations, the temperature experienced by buds must be lower to promote any acclimation. Both

parameters *b* and *c* are shared with deacclimation potential, which is explained further below (in ***2.4.2. Deacclimation***).

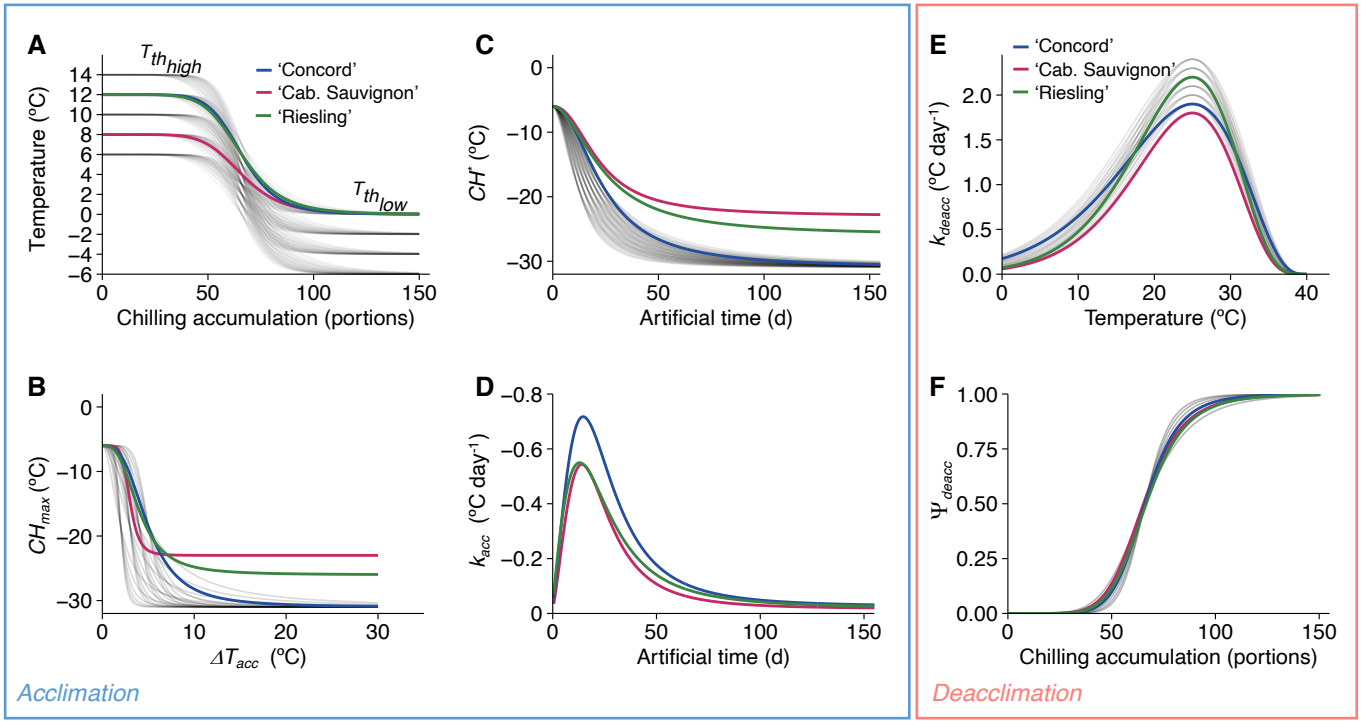

Figure 1. Graphic representation of functions used to model cold hardiness of grapevine buds for 'Concord', 'Cabernet Sauvignon', and 'Riesling'. Functions are separated between acclimation (**A-D**) and deacclimation (**E, F**). Solid colored lines represent fits (**A, B, E, F**), or example fits for each cultivar (**C, D**); blue = 'Concord', magenta = 'Cabernet Sauvignon', green = "Riesling'. The semi-transparent grey lines represent iterations of combinations for 'Concord' parameters that were not selected. **(A)** Acclimation step 1; see also **Eq. 2**. The temperature below which acclimation occurs is the acclimation temperature threshold ($T_{th_{acc}}$), which changes according to chill accumulation. As chill accumulates, $T_{th_{acc}}$ changes from high acclimation temperature threshold ($T_{th_{high}}$) to low acclimation temperature threshold ($T_{th_{low}}$). The driver of acclimation, *DT*, is calculated from the difference between the daily low temperature and $T_{th_{acc}}$. **(B)** Acclimation step 2; see also **Eq. 3**. Upper limit of curves, or maximum cold hardiness (CH_{max}) at DT_{acc} = 0°C, represents cold hardiness at bud set ($CH_{bud\ set}$), which was fixed at –6 ºC for all cultivars. Lower limit of curves, or CH_{max} at DT_{acc} = 30°C, represents the maximum cold hardiness observed during any season ($CH_{abs\ max}$), which we set equal to the average of the 15 lowest cold hardiness measurements rounded down to the nearest integer. The shape of these curves between the upper and lower limits are determined by fitting the slope (*d*) and intercept (*f*) parameters in **Eq. 3**. **(C)** Acclimation step 3; see also **Eq. 4**. Example curves for artificial cold hardiness (CH^*) for a maximized *DT* in response to artificial time. These curves represent the time buds would take when exposed to a given DT_{acc} to reach the CH_{max} elicited. **(D)** Final acclimation rate based on partial derivative of step 3; see also **Eq. 5**. The acclimation rate k_{acc} is obtained based on the artificial time calculated from Eq. 4 solved for time using the the cold hardiness of the previous day as CH^*. **I** Deacclimation step 1, deacclimation rate; see also **Eq. 6**. The deacclimation rate (k_{deacc}) varies across temperature from 0 °C to 40°C. For all cultivars, k_{deacc} reaches maximum at 25 °C (T_{optim}) and is zero at 40 °C (T_{max}). Two aspects that were fit separately for each cultivar are the maximum deacclimation rate ($k_{deacc_{max}}$) and the coefficient *a*, which determines the slope on either side of $k_{deacc_{max}}$. **(F)** Deacclimation step 2, deacclimation potential; see also **Eq. 7**. Deacclimation potential (Y_{deacc}) modulates the deacclimation rate to an effective deacclimation rate (k^*_{deacc}) based on chill accumulation from low to high (i.e., Y_{deacc} increases as chill accumulates). The inflection point for all cultivars was fixed at 66 chill portions, while the slope parameter of Y_{deacc} curves (*b*) was fit separately for each cultivar and is shared with $T_{th_{acc}}$.

The second function describes the maximum cold hardiness possible (CH_{max}) elicited by the difference between the T_{min} of any given day and the $T_{th_{acc}}$ ($\Delta T_{acc} = T_{th_{acc}} - T_{min}$). Here, we used a log-logistic function to describe the response:

$$CH_{max}\,(\Delta T_{acc}) = CH_{bud\ set} + {(CH_{abs\ max} - CH_{bud\ set})}/{1 + e^{[d\,(\ln(\Delta T_{acc}) - \ln(f))]}} \quad [Eq.\,3]$$

where $CH_{bud\ set}$ is the minimum cold hardiness, which was conservatively fixed at –6 ºC for all cultivars (the resolution of the limit of detection of our equipment); $CH_{abs\ max}$ is the maximum cold hardiness observed during any season, and here was used as the average of the 15 lowest cold hardiness measurements rounded down to the nearest integer; d is the slope associated with the logistic curve; and f is the inflection point of the logistic curve (**Fig. 1B**).

The third function describes the rate of acclimation based on how close to the CH_{max} the cold hardiness of the previous day ($CH_{t_{i-1}}$) is. For simplicity, here we present this in two steps. First, the shift from $CH_{bud\ set}$ to the CH_{max} elicited by any given ΔT_{acc} is not instant. Should buds be exposed to a constant ΔT_{acc}, acclimation would occur over time, giving rise to rate of acclimation. Because these are based on assumptions related to acclimation rather than experiments, we have dubbed this cold hardiness as an artificial cold hardiness (CH^*). The artificial cold hardiness (CH^*) thus changes from $CH_{bud\ set}$ to CH_{max} as a function of time based on a log-logistic function:

$$CH^* = CH_{bud\ set} + {(CH_{max} - CH_{bud\ set})}/{1 + e^{\{g\,[\ln(t) - \ln(h)]\}}} \quad [Eq.\,4]$$

where g and h are the slope and intercept associated with a log-logistic curve (**Fig. 1C**). CH^* is also indirectly a function of the temperature and chill accumulation since both contribute to defining CH_{max}. An artificial time t_a is found by solving **Eq. 4** for t using $CH^* = CH_{t_{i-1}}$ (the cold hardiness of the previous day) and CH_{max} for T_{min} at t_i (using **Eq. 3**). Using t_a, we can obtain the rate of acclimation (k_{acc}) in the field at any time t_i through the partial derivative of the log logistic function with respect to time:

$$k_{acc} = (CH_{max} - CH_{bud\ set}) \times \left\{0.001 + \frac{\left(e^{[g\ (\ln(t_a)-\ln(h))]}\right) \times (-g/t_a)}{(1 + e^{[g\ (\ln(t_a)-\ln(h))]})^2}\right\} \quad [Eq.5]$$

Where g and h are the slope and intercept associated with a log-logistic curve, and t_a is the artificial time based on $CH_{t_{i-1}}$ (**Fig. 1D**). Here, k_{acc} is a function of artificial time (since field temperature changes continuously), and the field temperature and accumulated chill that define CH_{max}. In addition to the rate obtained through the partial derivative, a 0.001 (or 0.1%) rate was added to acclimation at all times. This was incorporated to acknowledge anecdotal observations that buds seem to continue acclimating when temperatures are very low (Kovaleski personal observations). Therefore, buds can surpass the CH_{max} elicited by any ΔT_{acc}, and even a cultivar's $CH_{abs\ max}$, if temperatures are continuously low. While the actual effect of the factor is very small in this model, the factor could be enhanced or reduced to accommodate new perspectives based on future research. A sample workflow of an *Acclimation* step is shown in **Fig. 2**.

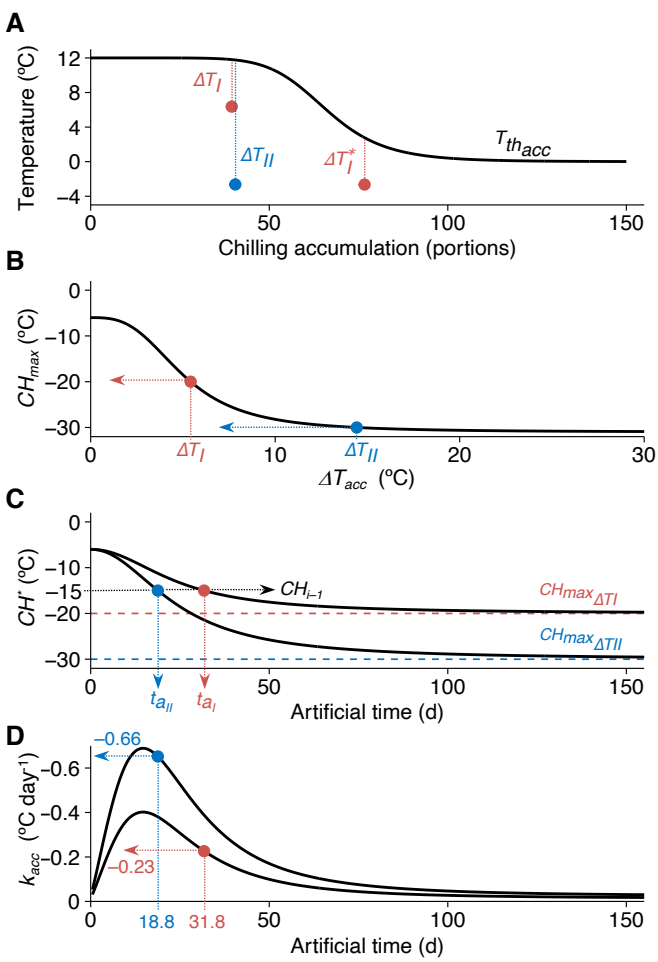

Figure 2. Example workflow to describe progression for acclimation step in the NYUS.1 model and highlight relative importance of changes in conditions. **(A)** The $T_{th_{acc}}$ in this example varies from 12 ºC ($T_{th_{low}}$) to 0 ºC ($T_{th_{high}}$) across accumulating chill. *DT* is the difference between T_{min} (points) and $T_{th_{acc}}$. Two DT_{acc} scenarios are included in this example (DT_I and DT_{II}) to highlight importance of conditional changes throughout acclimation calculations. Here we observe that different temperatures can lead to the same *DT* ($DT_I = DT^*_I$): as chill accumulates and $T_{th_{acc}}$ decreases, a lower T_{min} would elicit the same response. We can also observe that the same temperature can lead to different *DTs* ($DT_{II} \neq DT^*_I$) if at two different chilling accumulations. **(B)** Based on a given DT_{acc}, a certain CH_{max} is obtained, which is greater (in magnitude) for greater DT_{acc}. **(C)** With the different CH_{max} for each of the scenarios, DT_I and DT_{II}, we can observe the different curves for gains in cold hardiness if buds were constantly exposed to those temperatures. Solving ***Eq. 4*** for time using the *CH* of the previous day (CH_{i-1}), here –15 ºC, as CH^* we obtain the time at which this would occur along that artificial temperature exposure: t_{a_I} and $t_{a_{II}}$. **(D)** Using the first derivative of those acclimation curves, we obtain the curves for rate of acclimation, k_{acc}. The rate of acclimation for a given day, t_i, is calculated by solving ***Eq. 5*** using t_{a_I} and $t_{a_{II}}$.

2.4.2. For ***Deacclimation***, two functions were used (**Figs. 1E, F**) which are based on descriptions from previous empirical experiments on grapevines and other species (Kovaleski et al., 2018; Kovaleski, 2022; North et al., 2022). One is for the rate of deacclimation (k_{deacc}) that any given temperature elicits. Other functions have been used to describe k_{deacc}, such as a logistic (Chuine, 2000; North et al., 2022), combination of exponential and logarithmic (Kovaleski et al. 2018) or a third-degree polynomial (Kovaleski, 2022). Here, the temperature response curve used was that based on a temperature-photosynthesis curve (O'Neil et al., 1972):

$$k_{deacc}(T) = k_{deacc_{max}} \left(\frac{T_{max} - T}{T_{max} - T_{opt}} \right)^{a} \times e^{\left[a \left\{1 - \left(\frac{T_{max} - T}{T_{max} - T_{opt}}\right)\right\}\right]} \quad [Eq. 6]$$

where k_{deacc} (T) is the rate of deacclimation (°C day^{-1}) at temperature T (°C); a is a coefficient related to the slope of the curve; $k_{deacc_{max}}$ is the maximum rate of deacclimation at the optimal temperature (T_{optim}, °C), and T_{max} is the maximum temperature (°C) from which point the deacclimation rate becomes zero. T_{optim} and T_{max} were fixed at 25 °C and 40 °C, respectively. While an absolute decrease in rates with temperature has not observed in empirical studies (Kovaleski et al., 2018; North et al., 2022), some considerations can be made: a deviation from exponential increase in rates was observed (Kovaleski et al., 2018; Kovaleski, 2022); temperatures much higher than 25 °C do not occur frequently during the deacclimation period in the spring; and the suggestion of deacclimation as an enzymatic process is acknowledged by this curve (Kalberer, 2006; Kovaleski et al., 2018). The T_{optim} of 25 °C was used based on previously reported deacclimation rates (Kovaleski et al., 2018; North et al., 2022). Because of the non-linearity of the response, the amount of deacclimation observed in a day was the average between k_{deacc} for the daily T_{max} and T_{min}, rather than using the average of the temperature.

The second function defining deacclimation is the deacclimation potential (Ψ_{deacc}), which modulates the level of effective deacclimation occurring based on a log logistic function of chill accumulation during the winter:

$$\Psi_{deacc}(chill) = {}^{1}/_{1 + e^{[-b\,(\ln(chill) - \ln(c)]}} \quad [Eq. 7]$$

where b is the slope associated with the log-logistic curve, and c is the inflection point of the log-logistic curve, a chilling requirement-analogous measurement where 50% of the maximum Ψ_{deacc} is achieved. Because b and c were shared with $T_{th_{acc}}$, such that the dormancy-related responses to *chill* are symmetric for *Acclimation* and *Deacclimation*, a negative sign is used for b here (negative values indicate increases in Ψ_{deacc} as chill accumulation increases). For c, a fixed value of 66 chill portions was used based on previous work with many species (Kovaleski, 2022). The phased integration of *Acclimation* and *Deacclimation* provided by the shared b and c terms mean that as chilling accumulates, *Acclimation* becomes more difficult, requiring lower temperatures, while *Deacclimation* becomes more pronounced.

The effective deacclimation rate at any time t_i, $k^*_{deacc_{t_i}}$, is ultimately a result of the product of the average daily deacclimation rate and the deacclimation potential:

$$k^*_{deacc_{t_i}} = {[k_{deacc}\,(T_{min}) + k_{deacc}\,(T_{max})]}/{2} \times \Psi_{deacc} \quad [Eq.8]$$

2.5. Model optimization. The cold hardiness data available was separated in calibration and validation datasets by season-year. The ratio was approximately 2/3 calibration and 1/3 validation. The years were randomly assigned to each dataset within each cultivar using set.seed() based on when code preparation for each cultivar started [17 August for 'Concord' set.seed(1708); 7 June for 'Cabernet Sauvignon' set.seed(0706); 7 July for 'Riesling' set.seed(0708)]. The dynamic model based on **Eq. 1** predicts cold hardiness with 1-day time steps. Nine parameters were optimized here: $T_{th_{low}}$, $T_{th_{high}}$, b, d, f, g, h, $k_{deacc_{max}}$, and a (see **Table 1** and **Fig. 1**). The parameters were optimized using a stepwise iterative method based on the minimization of root mean square error (RMSE) between predicted and observed CH for a calibration dataset ($RMSE_{cal}$). The parameter combination with lowest $RMSE_{cal}$ was then used to predict CH using a naïve validation dataset, and RMSE of a prediction was then calculated ($RMSE_{val}$). The $RMSE_{val}$ of the present model was compared to that of the predictions based on the latest update of the currently available grapevine bud cold hardiness developed in Washington state, WAUS.2 ($RMSE_{WA}$; Ferguson et al., 2014 – see also Ferguson et al., 2011 for details on equations). Other fitness statistics were also calculated for both models [$Bias = CH_{measured} - CH_{predicted}$; Pearson correlation ($r$)].

Table 1. Parameter levels tested in all combinations stepwise for three grapevine cultivars for each of six equations. A total of 3,386,880 combinations were tested per cultivar for all years in the calibration datasets.

Cultivar	$T_{th_{low}}$	$T_{th_{high}}$	b	c	$CH_{abs\ max}$			$CH_{bud\ set}$	d	f	g	h	k_{deacc}			a
					Con	CS	Rie						Con	CS	Rie	
Start	–6	6	6	66	31	23	2	6	2	2	–2.3	12	1.9	1.3	1.7	3.5
Stop	0	14	11	66	31	23	7	6	7	5	–1.7	24	2.4	1.8	2.2	5.0
Step	2	2	1	0	0			0	1	1	0.1	2	0.1			0.5
n	4	5	6	1	1			1	6	4	7	7	6			4
Equation	**Eq. 2**		**Eqs. 2, 7**		**Eq. 3**			**Eqs. 1, 3, 4, 5**	**Eq. 3**		**Eqs. 4, 5**		**Eq. 6**			

3. Results

The NYUS.1 model proposed here using optimized parameters for each cultivar based on calibration dataset (**Table 2**, **Fig. 1**) produced good predictions of cold hardiness for the validation dataset of the three cultivars studied ($RMSE_{val}$ ranging from 2.12 ºC to 2.72 ºC, bias from –1.46 ºC to 1.28 ºC; **Table 2**, **Figs. 3 and 4A**).

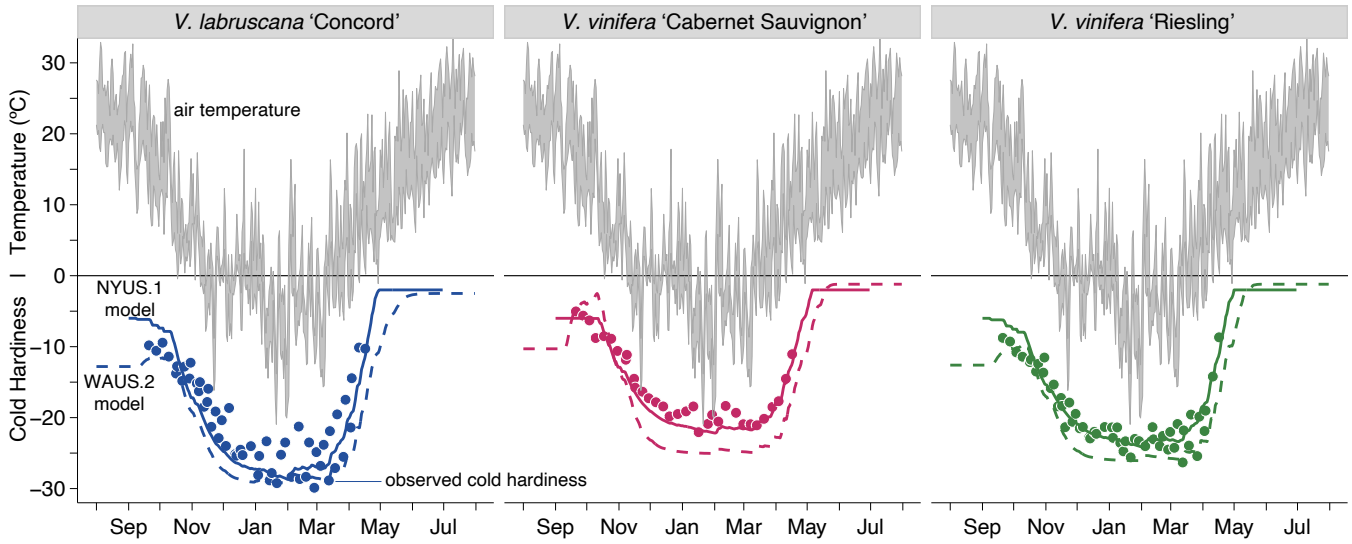

Figure 3. Observed cold hardiness, based on average low temperature exotherms (points), plotted with predicted bud cold hardiness according to NYUS.1 model (solid lines) and WAUS.2 model (dashed lines) with daily maximum and minimum temperature range (grey ribbons) in 2018-2019 for three grapevine cultivars.

The values for $RMSE_{cal}$ (2.09 ºC, 1.47 ºC, 1.61 ºC for 'Concord', 'Cabernet Sauvignon', and 'Riesling', respectively) and $RMSE_{val}$ (**Fig. 4A**) were similar within each cultivar. This demonstrates the model and parameters chosen are robust, thus predicting similar variability in both datasets, dealing well with the year-to-year weather variations. In absolute values, predictions produced were slightly better for the two *V. vinifera* cultivars compared to 'Concord'. This may be a result of the higher responsiveness of 'Concord' compared to either *V. vinifera* (greater changes in *CH* over time), as well as its overall greater cold hardiness.

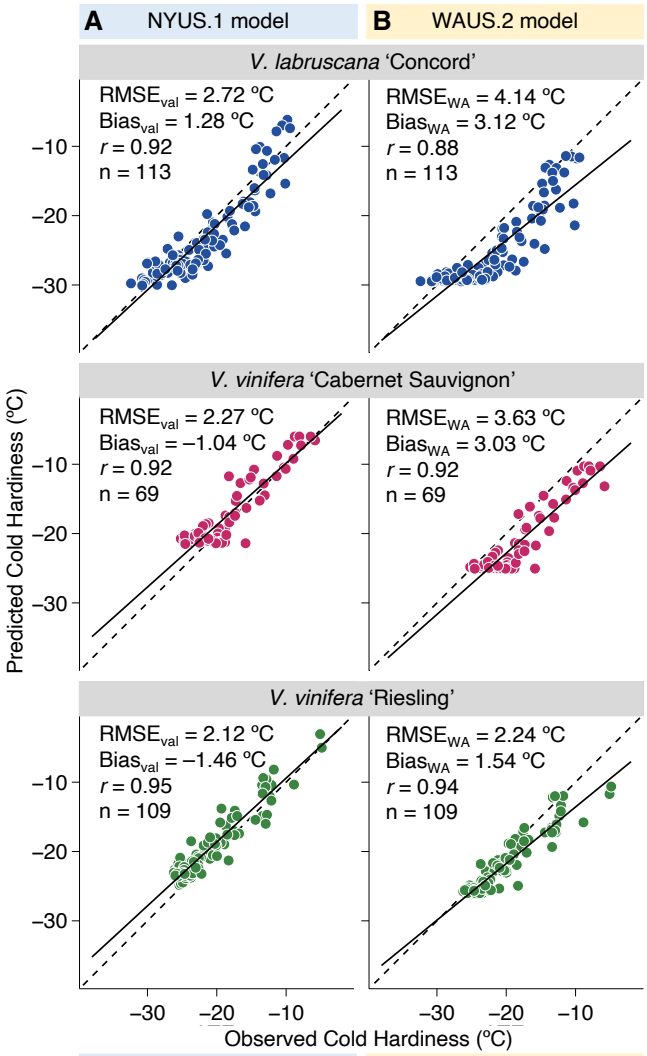

Figure 4. Comparison between predicted and observed bud cold hardiness, reported as average low temperature exotherm (LT_{50}), for three grapevine cultivars using both the (**A**) NYUS.1 model and (**B**) WAUS.2 model. Statistics are listed in each panel, including root mean square error (RMSE), bias, correlation coefficient (r), and sample size (n). The prediction and observation correlations are illustrated (solid black line) along with a one-to-one reference (dashed black line).

Compared to the existing model, WAUS.2, the newly developed NYUS.1 model produced better predictions for 'Concord' and 'Cabernet Sauvignon', and slightly better or comparable predictions for 'Riesling' for data from Geneva, NY (**Figs. 3,4**). $RMSE_{WA}$ was only computed within the validation

datasets, and had values of 4.14 ºC, 3.63 ºC, and 2.24 ºC for 'Concord', 'Cabernet Sauvignon', and 'Riesling', respectively.

The WAUS.2 model consistently overpredicted cold hardiness ($Bias_{WA}$ of 3.12 °C, 3.03 °C, and 1.54 °C for 'Concord', 'Cabernet Sauvignon', and 'Riesling', respectively; **Fig. 4B**). This is likely due to the development of the model using data from a region with relatively warmer and drier winters. The bias may be enhanced by the WAUS.2 model's design, where any temperature below the temperature threshold that separates acclimation and deacclimation can lead to full acclimation to the maximum cold hardiness. In the present model, low temperatures have both a different maximum cold hardiness possible (**Eqs. 2 and 3**) and different acclimation rates (due to the effect of maximum cold hardiness on **Eqs. 4 and 5**). Our model, although selected based on lowest $RMSE_{cal}$, also had low bias for the three cultivars.

In the same season, 'Concord' gains more cold hardiness, and does so faster, than the two *V. vinifera* despite the same starting cold hardiness. This effect is observed in the generally lower CH_{max} (**Fig. 1B**) and higher rates of acclimation in response to ΔT_{acc} (**Fig. 1D**). 'Concord' also loses its cold hardiness faster than the *V. vinifera*, while 'Riesling' is also faster than 'Cab. Sauvignon'. Within the optimized parameters, 'Riesling' has a higher $k_{deacc_{max}}$ than 'Concord'. However, because of the higher a parameter for **Eq. 6** (**Table 2**), 'Riesling' has lower deacclimation rates at temperatures between 0 ºC and 17.5 ºC (**Fig. 1E**), which are temperatures that largely predominate during the spring, when the majority of deacclimation occurs.

While all combinations of parameters were tested for optimization within each cultivar, some parameters were found to be very similar between the cultivars for the NYUS.1 model. This could suggest that the model is realistic in describing a physiological process that is conserved among the different cultivars within a species ('Cabernet Sauvignon' and 'Riesling'), and among grapevine species (here *V. vinifera* and *V. labruscana*). 'Cabernet Sauvignon' had a lower $T_{th_{high}}$ than 'Concord' and 'Riesling', but the rate of change in $T_{th_{acc}}$ in response to chilling (b) was very similar. The parameter b, which defines the slope of the log-logistic associated here with both $T_{th_{acc}}$ and Ψ_{deacc}, has previously been suggested to be the same for all species for deacclimation (Kovaleski, 2022), leaving regulation of magnitudes of deacclimation (effective deacclimation) to the effect of temperature alone on the rate of deacclimation, k_{deacc}.

Table 2. Parameter value combinations that minimize root mean square error for three grapevine cultivars in calibration datasets. Years used in calibration and validation datasets.

Cultivar	$T_{th_{low}}$	$T_{th_{high}}$	b	c	$CH_{abs\ max}$	$CH_{bud\ set}$	d	f	g	h	k_{deacc}	a	Calibration	Validation
'Concord'	0	12	8	66	–31	–6	3	5	–2.1	24	1.9	3.5	2012-2013, 2013-2014, 2016-2017, 2017-2018, 2019-2020	2014-2015, 2018-2019, 2020-2021
'Cabernet Sauvignon'	0	8	7	66	–23	–6	6	3	–2.2	22	1.8	5.0	2016-2017, 2017-2018, 2018-2019, 2020-2021	2015-2016, 2019-2020
'Riesling'	0	12	7	66	–26	–6	3	4	–1.9	24	2.2	5.0	2012-2013, 2014-2015, 2017-2018, 2018-2019, 2019-2020, 2020-2021	2013-2014, 2015-2016, 2016-2017

4. Discussion

Accurate modeling of cold hardiness is an important step in understanding adaptation of species and cultivars in future climates (Wolkovich et al., 2018; Körner, 2021). However, modeling of this trait is also helpful for growers in guiding management practices and in cultivar choice for different regions in current climates. Here we used known deacclimation responses (Kovaleski et al., 2018; Kovaleski, 2022; North et al., 2022) and posited acclimation responses, along with a medium-term dataset with three cultivars that have relatively different cold hardiness behaviors to create a new cold hardiness prediction model for grapevine buds.

Our new model (NYUS.1 model) outperforms the currently available model for grapevine cold hardiness (WAUS.2; Ferguson et al., 2014) using New York state data. The WAUS.2 model consistently overestimates bud cold hardiness in New York, which consequently can underestimate freeze injury risk and occurrence. An overestimated cold hardiness could mislead adaptation of production systems (e.g. site selection or cultivar evaluation) and management decisions (e.g. spring pruning decisions). This is especially consequential as extreme and erratic weather events during winter become more frequent under changing climates (Casson et al., 2019; IPCC, 2022).

Parameters here are optimized using field data, as in other modeling studies (Ferguson et al., 2011; Ferguson et al., 2014; North et al., 2021). This was done despite some data available on experimentally determined deacclimation rates for the two *V. vinifera* cultivars (Kovaleski et al., 2018) and a few hybrids (North et al., 2022), though not 'Concord'. However, the estimated deacclimation rates based on **Eq. 6** for either *V. vinifera* cultivars were comparable to values previously reported (Kovaleski et al., 2018). This indicates field data, associated with models that prioritize the realism model dimension, can estimate parameters equivalent to controlled experiments.

The modulation of acclimation rate based on a logistic regression in response to time has a similar effect here as that of the Theta (θ) term in the WAUS.2 model, effectively attenuating the approach to any given cold hardiness. However, because each temperature elicits a different cold hardiness in our model (**Eqs. 2 and 3**), this effect is dynamic and can occur at any cold hardiness and any temperature, rather than just the asymptotical approach to absolute maximum and minimum cold hardiness as in Ferguson et al. (2014). This may improve the generalizability of our model in applications to regions other than New York. Deployment of the model to various cold hardiness monitoring programs (e.g., MI, PA, OH, CO, and Canada) for validation of fit would enable validation of these assumptions. Given that recent studies (Kovaleski et al., 2018; Kovaleski, 2022; North et al., 2022; North and Kovaleski, 2022) have demonstrated that cold hardiness status (as measured with DTA) is lost prior to budbreak, further development in cold hardiness models [e.g., adding a cold hardiness where budbreak is observed (Kovaleski et al., 2022)] could lead to tests using budbreak phenology datasets in regions where cold hardiness is not monitored as well.

The optimized $T_{th_{low}}$ was 0 ºC for all cultivars, which is the upper limit established. For a best fit of the model, it would be ideal to increase the range for iterations such that RMSE may be further minimized, ideally finding a global minimum. However, a higher $T_{th_{low}}$ would mean that the small deacclimations that happen at low but positive temperatures might have been counterbalanced by the effect of acclimation. By limiting $T_{th_{low}}$ to 0 ºC we prevented this effect, which would otherwise be particularly consequential during the spring when plants are fully chilled. Should data be gathered in warmer regions with lower seasonal chill accumulation, this limit should be evaluated and possibly be re-parameterized to remove these effects.

The calibration and validation datasets were not the same for all cultivars (**Table 2**; **Supplementary Figs. 1-3**). This was due to data not having been collected the same number of years for all cultivars. However, enough variation in the years available for the three cultivars appear to allow for good parameterization of the models. For example, within the calibration dataset for 'Concord', 2012-2013 is a much milder winter both in minimum temperature and the length of exposure to very low temperatures as compared to 2013-2014 (**Supplementary Fig. 1**).

Here, the transition of endodormancy to ecodormancy occurs quantitatively through the accumulation of chill that modulates the rates of deacclimation (k_{deacc}) through the deacclimation potential (Ψ_{deacc}). This is very different from the WAUS.1 and WAUS.2 models, where a qualitative transition occurs. It is likely that a qualitative transition works well as an assumption within a single region, given some regularity in the level of chill accumulation across years. However, for a single model to accomplish the estimation of deacclimation rates in regions of lower chill accumulation and higher chill accumulation, a quantitative transition is required based on experimental results (Kovaleski et al., 2018; Kovaleski, 2022, North et al., 2022). Field data from different regions, particularly those where low chilling accumulation occur will be required to test this. It is also important to note that some management practices that "supplement chilling" and break dormancy (e.g., application of hydrogen cyanamide) have not been studied from a cold hardiness context, and therefore we do not expect the model to excel if applied to regions where such treatments occur until effects of dormancy breaking treatments has been studied.

The dynamic model was used here to estimate chilling accumulation, due to its reported higher transferability to warmer environments (Luedeling and Brown, 2011). Within high chill accumulation regions, it has been reported to be highly correlated to other chilling models, such as "Utah" (Richardson et al., 1974) and "North Carolina" (Shaltout and Unrath, 1983) [e.g., in Boston, MA, USA (Kovaleski, 2022), and Madison, WI, USA (North et al., 2022)]. However, it is still possible that all chill models are incorrectly describing chilling accumulation, and therefore this may be a source of error for predictions, especially in regions with low chill accumulation. Deacclimation experiments, such as in other studies by the present authors (Kovaleski et al., 2018; Kovaleski, 2022; North et al., 2022), that use material collected from warmer climates should help elucidate the dynamics of chilling. Should the chilling accumulation models change, parameter changes within the model presented here may be required.

In our calibration dataset, the rounded average of the 15 most cold hardy points for 'Concord' is –31 ºC, and the lowest observed cold hardiness was –31.4 ºC. This is below the maximum possible using the WAUS.2 model for that cultivar (–29.5 ºC). This suggests the maximum cold hardiness for this genotype may not be achieved in Washington's conditions, which are relatively warmer compared to upstate New York. The higher value of cold hardiness being the maximum possible in their model results in a hard limit seen in the lower end of the observed vs. predicted plots for the WAUS.2 model (**Fig. 4B**). The opposite is observed in 'Cabernet Sauvignon', however, where the present model uses a maximum cold hardiness of –23 ºC (although this value would be –26 ºC if estimated from the validation dataset), whereas the Washington model uses a value of –25.1 ºC. In the currently proposed model, besides having a lower maximum, this is not a hard limit given the possibility of a low acclimation rate at any temperature.

The values estimated for the slope associated with the log logistic for chill responses were similar to those previously reported (Kovaleski, 2022). Here, both acclimation and deacclimation were guided by the same slope, providing the phased integration of both, which may have led to slight differences from measured effects. Future studies in acclimation could help understand whether the response should be maintained as varying alongside deacclimation or not.

The similarity in parameter values across cultivars for acclimation and deacclimation, particularly the portions that *do not describe magnitude* (i.e., slope for $T_{th_{acc}}$, slope and intercept for CH^*, and slope for Ψ_{deacc}), suggests a conserved physiology if the present model (NYUS.1) is correctly approximating responses. This has been suggested for the dormancy and deacclimation across the land plant phylogeny (Kovaleski, 2022), though without using multiple genotypes within a species. Deacclimation appears to be a simpler process, where no temperature sensing is required, only temperature perception (Penfield, 2008). It remains to be tested whether acclimation has conserved mechanisms that can easily translate to mathematical models of the process, though acclimation appears to be more difficult to describe and elicit in controlled environment experiments.

Variability in model performance across regions is at least partially a consequence of model development with datasets from a single region. However, there is a lack of freely available datasets of cold hardiness from different climates that restricts improvements in model development, unlike with other types of data such as spring phenology (e.g., Pan European Phenology Project and USA's National

Phenology Network). Therefore, we are making our dataset public so other efforts may use this medium-term dataset (https://github.com/apkovaleski/NYUS.1_CHmodel; Kovaleski et al., 2022). It is also noticeable that most cold hardiness datasets are produced in higher latitudes and temperate climates where considerably low temperatures occur during winter [e.g., Washington (Ferguson et al., 2014), Wisconsin (North et al., 2021, 2022) and New York states within the US; Chile (Rubio and Pérez, 2020)]. There is a need for new data to be collected from warmer locations in lower latitudes such that parameters can be optimized based on warmer subtropical (or even tropical) climates. It is possible that the model proposed here, the existing WAUS.2 model (Ferguson et al., 2014), or regional adaptations (North et al., 2021) perform variably across different regions, and therefore models should continue to be used in conjunction in new regions to validate and tune predictions. As models continue to be improved, convergence of responses should result in high confidence of predictions.

Our model uses only air temperature-related parameters to describe cold hardiness. Some variation in cold hardiness can also be explained by temperature mediated aspects of microclimate and daylength, such as through radiative warming (Grace, 2006; Quiñones et al., 2019; Vitasse et al., 2021), wind (Grace, 2006), water availability, and daily amplitude in temperature (Gonzalez Antivilo et al., 2017; Matsubara 2018). In addition to direct effects on cold hardiness, such factors may indirectly affect cold hardiness through effects on dormancy. However, integrating these relatively minor factors influencing cold hardiness changes into models, while reducing prediction error somewhat, also increase a model's computational complexity and potentially make the results of parameter computing less generalizable.

5. Conclusions

The NYUS.1 model produced here demonstrates a robust manner of predicting cold hardiness for buds of three different grapevine cultivars. This model integrates novel deacclimation concepts discussed in recent literature (Kovaleski et al., 2018; Kovaleski, 2022; North et al., 2022). It is possible that future research regarding acclimation could lead to a better understanding of the processes leading to gains in cold hardiness and subsequently improved modeling approaches. However, acclimation seems to be an elusive process to date and coincides with other significant physiological changes that are only partially understood (e.g., dormancy induction). Therefore, further research in acclimation and cold hardiness modeling will need to continually assess the balance between model realism and model accuracy. The NYUS.1 model proposed here provides accurate cold hardiness predictions in the meantime and a

framework on which to build. Better predictions were produced using the NYUS.1 model when compared to the WAUS.2 model (Ferguson et al., 2014). Thus, the proposed model may be used in lieu of, or in addition to, existing models to aid in decision making steps. Despite having been developed using regional data, the selection of similar parameters across cultivars could indicate a representative description of physiological processes that may also promote transferability into other regions with some caveats, such as errors in chilling accumulation models.

Acknowledgements

We would like to thank Hanna Martens, Bill Wilsey, Lex Pike, and Kathleen Deys for help collecting and processing grape bud tissue for field cold hardiness measurements. We would also like to thank Ravines Vineyard in Geneva, NY for access to *V. vinifera* 'Cabernet Sauvignon' and 'Riesling' vines. This work was partially supported by the Office of the Vice Chancellor for Research and Graduate Education at the University of Wisconsin–Madison with funding from the Wisconsin Alumni Research Foundation, and through the USDA ARS appropriated project 1910-21220-006-00D.

Competing interests

The authors have no competing interests to declare.

Figure Legends

Figure 1. Graphic representation of functions used to model cold hardiness of grapevine buds for 'Concord', 'Cabernet Sauvignon', and 'Riesling'. Functions are separated between acclimation (**A-D**) and deacclimation (**E, F**). Solid colored lines represent fits (**A, B, E, F**), or example fits for each cultivar (**C, D**); blue = 'Concord', magenta = 'Cabernet Sauvignon', green = "Riesling'. The semi-transparent grey lines represent iterations of combinations for 'Concord' parameters that were not selected. **(A)** Acclimation step 1; see also **Eq. 2**. The temperature below which acclimation occurs is the acclimation temperature threshold ($T_{th_{acc}}$), which changes according to chill accumulation. As chill accumulates, $T_{th_{acc}}$ changes from high acclimation temperature threshold ($T_{th_{high}}$) to low acclimation temperature threshold ($T_{th_{low}}$). The driver of acclimation, ΔT, is calculated from the difference between the daily low temperature and $T_{th_{acc}}$. **(B)** Acclimation step 2; see also **Eq. 3**. Upper limit of curves, or maximum cold hardiness (CH_{max}) at ΔT_{acc} = 0°C, represents cold hardiness at bud set ($CH_{bud\ set}$), which was fixed at –6 ºC for all cultivars. Lower limit of curves, or CH_{max} at ΔT_{acc} = 30°C, represents the maximum cold hardiness observed during any season ($CH_{abs\ max}$), which we set equal to the average of the 15 lowest cold hardiness measurements rounded down to the nearest integer. The shape of these curves between the upper and lower limits are determined by fitting the slope (d) and intercept (f) parameters in **Eq. 3**. **(C)** Acclimation step 3; see also **Eq. 4**. Example curves for artificial cold hardiness (CH^*) for a maximized ΔT in response to artificial time. These curves represent the time buds would take when exposed to a given ΔT_{acc} to reach the CH_{max} elicited. **(D)** Final acclimation rate based on partial derivative of step 3; see also **Eq. 5**. The acclimation rate k_{acc} is obtained based on the artificial time calculated from Eq. 4 solved for time using the the cold hardiness of the previous day as CH^*. **I** Deacclimation step 1, deacclimation rate; see also **Eq. 6**. The deacclimation rate (k_{deacc}) varies across temperature from 0 °C to 40°C. For all cultivars, k_{deacc} reaches maximum at 25 °C (T_{optim}) and is zero at 40 °C (T_{max}). Two aspects that were fit separately for each cultivar are the maximum deacclimation rate ($k_{deacc_{max}}$) and the coefficient a, which determines the slope on either side of $k_{deacc_{max}}$. **(F)** Deacclimation step 2, deacclimation potential; see also **Eq. 7**. Deacclimation potential (Ψ_{deacc}) modulates the deacclimation rate to an effective deacclimation rate (k^*_{deacc}) based on chill accumulation from low to high (i.e., Ψ_{deacc} increases as chill accumulates). The inflection point for all cultivars was fixed at 66 chill portions, while the slope parameter of Ψ_{deacc} curves (b) was fit separately for each cultivar and is shared with $T_{th_{acc}}$.

Figure 2. Example workflow to describe progression for acclimation step in the NYUS.1 model and highlight relative importance of changes in conditions. **(A)** The $T_{th_{acc}}$ in this example varies from 12 ºC ($T_{th_{low}}$) to 0 ºC ($T_{th_{high}}$) across accumulating chill. ΔT is the difference between T_{min} (points) and $T_{th_{acc}}$. Two ΔT_{acc} scenarios are included in this example (ΔT_I and ΔT_{II}) to highlight importance of conditional changes throughout acclimation calculations. Here we observe that different temperatures can lead to the same ΔT ($\Delta T_I = \Delta T^*_I$): as chill accumulates and $T_{th_{acc}}$ decreases, a lower T_{min} would elicit the same response. We can also observe that the same temperature can lead to different ΔTs ($\Delta T_{II} \neq \Delta T^*_I$) if at two different chilling accumulations. **(B)** Based on a given ΔT_{acc}, a certain CH_{max} is obtained, which is greater (in magnitude) for greater ΔT_{acc}. **(C)** With the different CH_{max} for each of the scenarios, ΔT_I and ΔT_{II}, we can observe the different curves for gains in cold hardiness if buds were constantly exposed to those temperatures. Solving ***Eq. 4*** for time using the CH of the previous day (CH_{i-1}), here –15 ºC, as CH^* we obtain the time at which this would occur along that artificial temperature exposure: t_{a_I} and $t_{a_{II}}$. **(D)** Using the first derivative of those acclimation curves, we obtain the curves for rate of acclimation, k_{acc}. The rate of acclimation for a given day, t_i, is calculated by solving ***Eq. 5*** using t_{a_I} and $t_{a_{II}}$.

Figure 3. Observed cold hardiness, based on average low temperature exotherms (points), plotted with predicted bud cold hardiness according to NYUS.1 model (solid lines) and WAUS.2 model (dashed lines) with daily maximum and minimum temperature range (grey ribbons) in 2018-2019 for three grapevine cultivars.

Figure 4. Comparison between predicted and observed bud cold hardiness, reported as average low temperature exotherm (LT_{50}), for three grapevine cultivars using both the (**A**) NYUS.1 model and (**B**) WAUS.2 model. Statistics are listed in each panel, including root mean square error (RMSE), bias, correlation coefficient (r), and sample size (n). The prediction and observation correlations are illustrated (solid black line) along with a one-to-one reference (dashed black line).

Supplementary Figure Legends

Supplementary Figure 1. *Vitis labruscana* 'Concord' validation, calibration, and N/A datasets. Observed cold hardiness, based on average low temperature exotherms (blue points) plotted with predicted bud cold hardiness according to NYUS.1 model (solid blue lines) and WAUS.2 model (dashed blue lines) with daily maximum and minimum temperature range (grey ribbons).

Supplementary Figure 2. *Vitis vinifera* 'Cabernet Sauvignon' validation, calibration, and N/A datasets. Observed cold hardiness, based on average low temperature exotherms (magenta points) plotted with predicted bud cold hardiness according to NYUS.1 model (solid magenta lines) and WAUS.2 model (dashed magenta lines) with daily maximum and minimum temperature range (grey ribbons).

Supplementary Figure 3. *Vitis vinifera* 'Riesling' validation, calibration, and N/A datasets. Observed cold hardiness, based on average low temperature exotherms (green points) plotted with predicted bud cold hardiness according to NYUS.1 model (solid green lines) and WAUS.2 model (dashed green lines) with daily maximum and minimum temperature range (grey ribbons).

References

Arora R, Rowland LJ, Tanino K. 2003. Induction and Release of Bud Dormancy in Woody Perennials: A Science Comes of Age. *HortScience*. **38:** 911-921.

Casson NJ, Contosta AR, Burakowski EA, Campbell JL, Crandall MS, Creed IF, Eimers MC, Garlick S, Lutz DA, Morison MQ, Morzillo AT, Nelson SJ. 2019. Winter weather whiplash: Impacts of meteorological events misaligned with natural and human Systems in Seasonally Snow-Covered Regions. *Earth's Future.* **7:** 1434–1450.

Chuine I. 2000. A unified model for budburst of trees. *Journal of Theoretical Biology.* **207:** 337–347.

Cragin J, Serpe M, Keller M, Shellie K. 2017. Dormancy and cold hardiness transitions in winegrape cultivars Chardonnay and Cabernet Sauvignon. *American Journal of Enology and Viticulture.* **68**: 195–202.

Fennel A, Hoover E. 1991. Photoperiod influences growth, bud dormancy, and cold acclimation in *Vitis labruscana* and *V. riparia*. *Journal of the American Society for Horticultural Sciences*. **116:** 270-273.

Ferguson JC, Tarara JM, Mills LJ, Grove GG, Keller M. 2011. Dynamic thermal time model of cold hardiness for dormant grapevine buds. *Annals of Botany* **107**: 389–396.

Ferguson JC, Moyer MM, Mills LJ, Hoogenboom G, Keller M. 2014. Modeling dormant bud cold hardiness and budbreak in twenty-three *Vitis* genotypes reveals variation by region of origin. *American Journal of Enology and Viticulture.* **65**: 59–71.

Fishman S, Erez A, Couvillon GA. 1987a. The temperature dependence of dormancy breaking in plants: computer simulation of processes studied under controlled temperatures. *Journal of Theoretical Biology.* **126:** 309–321.

Fishman S, Erez A, Couvillon GA. 1987b. The temperature dependence of dormancy breaking in plants: mathematical analysis of a two-step model involving a cooperative transition. *Journal of Theoretical Biology.* **124**: 473–483.

Gonzalez Antivilo F, Paz RC, Keller M, Borgo R, Tognetti J, Juñent FR. 2017. Macro- and microclimate conditions may alter grapevine deacclimation: variation in thermal amplitude in two contrasting wine regions from North and South America. *International Journal of Biometeorology.* **61:** 2033-2045.

Grace J. 2006. The temperature of buds may be higher than you thought. *New Phytologist*. **170:** 1-3.

Hänninen H. 2013. Modeling bud dormancy release in trees from cool and temperate regions. *Acta Forestalia Fennica*. **213:** 47.

Hänninen H. 2016. Boreal and temperate trees in a changing climate: modelling the ecophysiology of seasonality. *Biometeorology.* Springer. https://doi.org/10.1007/978-94-017-7549-6.

IPCC. 2022. Climate Change 2022: impacts, adaptation, and vulnerability. contribution of working group II to the sixth assessment report of the intergovernmental panel on climate change [H.-O. Pörtner, D.C. Roberts, M. Tignor, E.S. Poloczanska, K. Mintenbeck, A. Alegría, M. Craig, S. Langsdorf, S. Löschke, V. Möller, A. Okem, B. Rama (eds.)]. Cambridge University Press. In Press.

Kalberer SR, Wisniewski M, Arora R. 2006. Deacclimation and reacclimation of cold-hardy plants: current understanding and emerging concepts. *Plant Science.* **171:** 3–16.

Körner C. 2021. The cold range limit of trees. *Trends in Ecology & Evolution.* **36:** 979-989.

Kovaleski AP. 2022. Woody species do not differ in dormancy progression: differences in time to budbreak due to forcing and cold hardiness. *Proceedings of the National Academy of Sciences of the United States of America* **119**: e2112250119.

Kovaleski AP, North MG, Martinson TE, Londo JP. 2022. Data from "Development of a new cold hardiness prediction model for grapevine using phased integration of acclimation and deacclimation responses" GitHub. https://github.com/apkovaleski/NYUS.1_CHmodel Deposited ## September 2022.

Kovaleski AP, Londo JP. 2019. Tempo of gene regulation in wild and cultivated Vitis species shows coordination between cold deacclimation and budbreak. *Plant Science*. **287:** 110178.

Kovaleski AP, Reisch BI, Londo JP. 2018. Deacclimation kinetics as a quantitative phenotype for delineating the dormancy transition and thermal efficiency for budbreak in *Vitis* species. *AoB Plants* **10**: ply066.

Kramer K, Leinonen I, Bartelink HH, Berbigier P, Borghetti M, Bernhofer C, Cienciala E, Dolman AJ, Froer O, Gracia CA, Granier A, Grünwald T, Hari P, Jans W, Kellomäki S, Loustau D, Magnani F, Markkanen T, Matteucci G, Mohren GMJ, Moors E, Nissinen A, Peltola H, Sabaté S, Sanchez A, Sontag M, Valentini R, Vesala T. 2002. Evaluation of six process-based forest growth models using eddy-covariance measurements of CO2 and H2O fluxes at six forest sites in Europe. *Global Change Biology.* **8:** 213-230.

Lang GA, Early JD, Martin GC, Darnell RL. 1987. Endo-, para-, and ecodormancy: physiological terminology and classification for dormancy research. *HortScience*. **22:** 371–377.

Levins R. 1966. The strategy of model building in population biology. *American Scientist.* **54:** 421-431.

Levins R. 1968. Evolution in changing environments: some theoretical explorations, Princeton University Press, 2020. *Project MUSE* https://muse.jhu.edu/book/73534.

Li S, Dami IE. 2016. Responses of *Vitis vinifera* 'Pinot gris' grapevines to exogenous abscisic acid (ABA): I. yield, fruit quality, dormancy, and freezing tolerance. *Journal of Plant Growth Regulation* **35:** 245–255.

Londo JP, Kovaleski AP. 2017. Characterization of wild North American grapevine cold hardiness using differential thermal analysis. *American Journal of Enology and Viticulture* **68**: 203–212.

Luedeling E. 2020. chillR: Statistical Methods for Phenology Analysis in Temperate Fruit Trees. R package version 0.70.24. https://CRAN.R-project.org/package=chillR .

Luedeling E, Brown PH. 2011. A global analysis of the comparability of winter chill models for fruit and nut trees. *International Journal of Biometeorology* **55**: 411–421.

Matsubara S. 2018. Growing plants in fluctuating environments: why bother? *Journal of Experimental Botany*. **69:** 4651-4654.

Mills LJ, Ferguson JC, Keller M. 2006. Cold-hardiness evaluation of grapevine buds and cane tissues. *American Journal of Enology and Viticulture.* **57:** 194–200.

North M, Kovaleski AP. 2022. Time to budbreak is not enough: cold hardiness evaluation is necessary in dormancy and spring phenology studies. *BioRxiv* (https://doi.org/10.1101/2022.09.15.508138).

North M, Workmaster BA, Atucha A. 2021. Cold hardiness of cold climate interspecific hybrid grapevines grown in a cold climate region. *American Journal of Enology and Viticulture* **72**: 318–327.

North M, Workmaster BA, Atucha A. 2022. Effects of chill unit accumulation and temperature on woody plant deacclimation kinetics. *Physiologia Plantarum* **174**: e13717.

Penfield S. 2008. Temperature perception and signal transduction. *New Phytologist.* **179:** 615-628.

Quiñones AJP, Keller M, Gutierrez MRS, Khot L, Hoogenboom G. 2019. Comparison between grapevine tissue temperature and air temperature. *Scientia Horticulturae* **247:** 407–420.

R Core Team. 2021. R: a language and environment for statistical computing. R Foundation for Statistical Computing, Vienna, Austria.

Richardson EA, Sceleu SD, Walker DR. 1974. A model for estimating the completion of rest for 'Redhaven' and 'Elberta' peach trees. *HortScience* **9**: 331–332.

RStudio Team. 2021. RStudio: integrated development environment for R. RStudio, PBC, Boston, MA.

Rubio S, Pérez FJ. 2020. Testing the Ferguson model for the cold-hardiness of dormant grapevine buds in a temperate and subtropical valley of Chile. *International Journal of Biometeorology* **64:** 1401–1408.

Schnabel BJ, Wample RL. 1987. Dormancy and cold hardiness in *Vitis vinifera* L. cv. White Riesling as influenced by photoperiod and temperature. *American Journal of Enology and Viticulture.* **38:** 265-272

Shaltout AD, Unrath CR. 1983. Rest completion prediction model for 'Starkimson delicious' apples. *Journal of the American Society for Horticultural Science* **108**: 957–961.

Shellie K, Kovaleski AP, Londo JP. 2018. Water deficit severity during berry development alters timing of dormancy transitions in wine grape cultivar Malbec. *Scientia Horticulturae.* **232:** 226-230.

USDA. 2019. 2017 Census of agriculture. United States. Summary and State Data. Vol. 1. Geographic Area Series.

Vitasse Y, Baumgarten F, Zohner CM, Kaewthongrach R, Fu YH, Walde MG, Moser B. 2021. Impact of microclimatic conditions and resource availability on spring and autumn phenology of temperate tree seedlings. *New Phytologist* **232:** 537–550.

Wolf TK, Pool RM. 1987. Factors affecting exotherm detection in the differential thermal analysis of grapevine dormant buds. *Journal of American Society for Horticultural Science.* **112:** 520-525.

Wolkovich EM, de Cortázar-Atauri IG, Morales-Castilla I, Nicholas KA, Lacombe T. 2018. From Pinot to Xinomavro in the world's future wine-growing regions. *Nature Climate Change.* **8:** 29-37.

Wolkovich EM, Auerbach J, Chamberlain CJ, Buonaiuto DM, Ettinger AK, Morales-Castilla I, Gelman A. 2021. A simple explanation for declining temperature sensitivity with warming. *Global Change Biology* **27:** 4947–4949.